RETRIEVAL OF FOREST WATER POTENTIAL FROM L-BAND VEGETATION OPTICAL DEPTH

T. Jagdhuber[1,2], A. Fluhrer[1,2], A.-S. Schmidt[1,2], F. Jonard[3,4], D. Chaparro[5], T. Meyer[4], N. Holtzman[6], A.G. Konings[6], A. Feldman[7], M. Baur[8], M. Piles[9] & D. Entekhabi[7]

[1]German Aerospace Center, Microwaves and Radar Institute, Muenchener Strasse 20, 82234 Wessling, Germany
[2]University of Augsburg, Institute of Geography, Alter Postweg 118, 86159 Augsburg, Germany
[3]Agrosphere (IBG-3), Institute of Bio- and Geosciences, Forschungszentrum Jülich GmbH,52428 Jülich, Germany
[4]Earth and Life Institute, Université catholique de Louvain, 1348 Louvain-la-Neuve, Belgium
[5]Universitat Politècnica de Catalunya, CommSensLab & IEEC/UPC, Jordi Girona 1-3, 08034 Barcelona, Spain
[6]Stanford University, Department of Earth System Science, 473 Via Ortega, Stanford, CA, USA.
[7]Massachusetts Institute of Technology, Department of Civil and Environmental Engineering, Vassar street 15, Cambridge, MA, USA.
[8]University of Cambridge, Department of Geography, Philippa Fawcett Dr, CB3 0AS, Cambridge, United Kingdom
[9]University of Valencia, Image Processing Lab, Parc científic, 46980 Paterna, Valencia, Spain
Email: {Thomas.Jagdhuber, Anke.Fluhrer, , Anne-Sophie.Schmidt}@dlr.de, {Francois.Jonard, Thomas.Meyer}@uclouvain.be, David.Chaparro@tsc.upc.edu, {nholtzma, konings}@stanford.edu., {afeld24, darae}@mit.edu, mjb311@cam.ac.uk, Maria.Piles@uv.es.

IGARSS 2021 - 2021 IEEE International Geoscience and Remote Sensing Symposium | 978-1-6654-0369-6/21/$31.00 ©2021 IEEE | DOI: 10.1109/IGARSS47720.2021.9554622

ABSTRACT

A retrieval methodology for forest water potential from ground-based L-band radiometry is proposed. It contains the estimation of the gravimetric and the relative water content of a forest stand and tests in situ- and model-based functions to transform these estimates into forest water potential.

The retrieval is based on vegetation optical depth data from a tower-based experiment of the SMAPVEX 19-21 campaign for the period from April to October 2019 at Harvard Forest, MA, USA. In addition, comparison and validation with in situ measurements on leaf and xylem water potential as well as on leaf wetness and complex permittivity are foreseen to understand limitations and potentials of the proposed approach. As a first result the radiometer-based water potential estimates of the forest stand are concurrent in time and similar in value with their in situ (xylem) counterparts from single trees in the radiometer footprint.

Index Terms— Soil plant atmosphere system, plant water potential, vegetation transmissivity, microwave radiometry, long wavelength, Harvard Forest.

1. INTRODUCTION

In contemporary space-borne microwave sensing, the observation of water filling states of different storage compartments (e.g. soil) is still the main focus of mission operations and application services [1]. In order to monitor water dynamics and fluxes (e.g. plant water uptake and transpiration rates) within the soil-plant-atmosphere system (SPAS), the saturation level and therefore the hydraulic potential, in units of pressure, needs to be observed. Van den Honert in 1948 [2] was among the first to recognize the analogy of current flow by Ohm's law with the water movement processes along SPAS. Thus, the hydraulic potential differences between single compartments in SPAS (e.g. vegetation and atmosphere) divided by the flow resistance enable the estimation of water fluxes, relevant for plant and ecosystem sciences.

As a starting point from microwave radiometry for water dynamics assessment, the vegetation optical depth (VOD) is provided quasi-operationally from brightness temperature observations by radiative transfer model-based inversion [3]. Encouragingly, a significant relationship of the L-band radiometer-derived VOD and the water potential of the xylem and the leaves of trees within a temperate forest stand was recently reported in [4]. In this research study, we use the database of [5], but aim at directly retrieving the forest water potential starting from VOD, as done in [6] for a wheat field.

2. TEST SITE AND EXPERIMENTAL DATA

The forest test site is located on Prospect Hill within Harvard Forest (42.535° N, 72.174° W), MA, USA. It is a temperate forest dominated by red Oak (*Quercus rubra*) formed by a humid continental climate [4]. As part of the SMAP Validation Experiment 2019-2021 (SMAPVEX 19 -21) campaign [7], in situ measurements for soil (moisture & temperature at 5 cm and 10 cm depth), trees (xylem permittivity and xylem water potential; leaf wetness and leaf water potential) and atmosphere (temperature) were conducted between April 28th and October 17th of 2019. Note that not all in situ data could be acquired continuously along the campaign period and an intensive measurement period with all sensors took place between 9th and 18th of July, 2019. The L-band (1.4 GHz) radiometer (Potter Horn, PR-1475, Radiometrics Inc.) was installed at 28 m height on a tower pointing with an incidence angle of 40° into the forest canopy with about 21 m to 23 m height. The footprint dimensions are 25 m by 20 m defined by the antenna's half power beam width (-3 dB) at 30° opening angle [5]. The instrument conducted hourly measurements of dual-polarimetric brightness temperature at an accuracy of approximately 2°K [8].

Only V-polarized measurements were used in this study, as H-polarized data showed 'unexplained fluctuations', as found previously in [4]. The dataset and further details on radiometer and in situ measurements are provided in [5] and [9].

The VOD-estimates, included in [5], were calculated using a single channel V-polarized (SCA-V) algorithm. Contrary to classical SCA-V in [3], in situ-based soil moisture is an input to the algorithm and the first order radiative transfer equation is solved for VOD. Since radiometer measurements were made at times where thermal equilibrium between soil and vegetation is not occurring, the soil and canopy temperatures were taken from in situ measurements. Instead of the canopy temperature, the air temperature at one-meter height at the forest stand was used, because direct canopy measurements were not available. This substitution was investigated in [4] and was shown to be valid.

For parameterization of soil roughness and scattering albedo, the standard values of the SMAP soil moisture product for temperate broadleaf forest were taken [4]. Figure 1 shows the VOD time series from 10th (noon) to 18th (11 pm) of July, 2019 during the intensive measuring period together with in situ data of xylem water potential [MPa], measured for one tree in the stand. The trend along time is at least two-fold, divided in a diurnal dynamic (driven by the solar cycle) and an overall decreasing trend (driven by hydrological dynamics) on multi-day to bi-weekly basis.

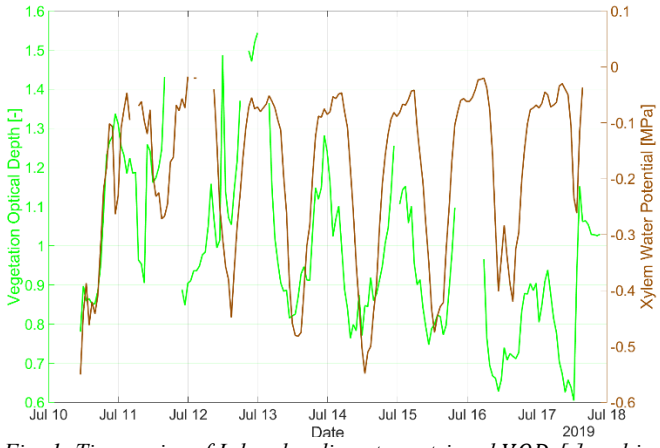

Fig. 1. Time series of L-band radiometer-retrieved VOD [-] and in situ-measured xylem water potential [MPa] of one tree in the temperate forest stand during an intensive measurement campaign in July 2019 at Prospect Hill (Harvard Forest) [5].

3. METHODOLOGY OF FOREST WATER POTENTIAL ESTIMATION

We first decompose VOD and extract the gravimetric water content of vegetation M_g, in kilogram water per kilogram wet biomass, as in [10]. It needs the vegetation height [m], the vegetation volume fraction [-], the main plant structure (e.g. vertically or randomly oriented), the major plant component (e.g. needles, discs, spheres) and the wavelength of the observing system [m] as input variables.

Next, the gravimetric water content is converted into the relative water content (RWC) using dry ($M_{g_{min}}$) and full turgor ($M_{g_{max}}$) references [11]:

$$RWC = \frac{M_g - M_{g_{min}}}{M_{g_{max}} - M_{g_{min}}} \cdot 100\ [\%]. \quad (1)$$

Afterwards, RWC is transformed into forest water potential (FWP), by a sigmoidal function of [12]:

$$FWP = \frac{FWP_{min}}{e^{\frac{-k_1 + RWC}{k_2}} + 1}\ [\text{MPa}], \quad (2)$$

where FWP_{min} is the minimum forest water potential of the RWC-FWP relationship. k_1 and k_2 are empirical parameters representing the inflection point and the rate of change between RWC and FWP

Parameterization of the sigmoidal function (k_1, k_2) is part of this study and is supported by in situ measurements, including RWC and water potential of leaves and branches at the forest site. Moreover, a variety of empirically derived functions could be used (see Fig. 2 in [13]). Figure 2 provides a first selection of applicable RWC-FWP relationships from in situ data [5] and models [12], [14] from (oak) forested environments.

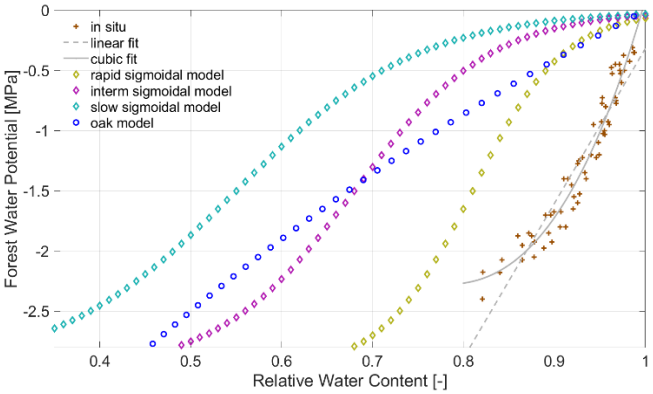

Fig. 2. Selection of applicable RWC-FWP relationships from in situ measurements [5] (brown crosses using different fits (dashed = linear, solid = cubic; all in gray color) and using models (sigmoidal [12] (diamonds), oak [14] (circles)).

4. FIRST RESULTS

Following the processing flow from VOD via M_g and RWC to FWP (see Section 2), we show results for the different intermediate variables and finally first estimates of FWP. Since these parameters are retrieved from tower-based L-band passive microwave remote-sensing observing the forest canopy under the reported acquisition scenario, they can only be considered as effective parameters compared to their in situ counterparts.

The retrieval of M_g is illustrated in Fig. 3 for the intensive measurement period (July 2019) and based on the assumption of a random needle permittivity model for calculating the canopy permittivity and an average vegetation height of 21 m

(top of canopy) from a product of [15]. As the vegetation volume fraction δ, seen by an L-band tower-based radiometer, is not known, a variety of volume fractions covering the wide range from 0.001 to 0.9 is applied.

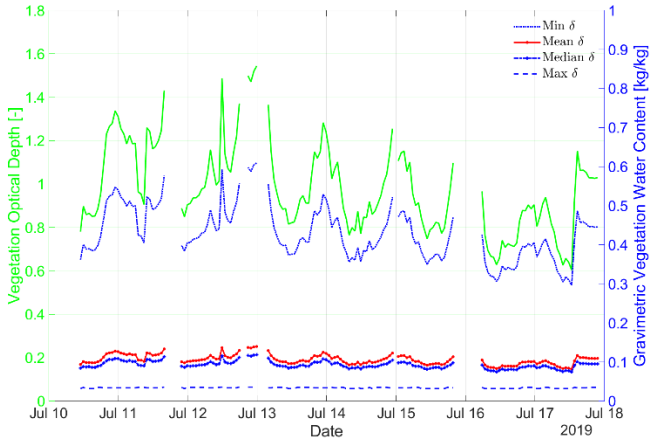

Fig. 3. Time series of M_g-estimates (blue color) compared to their retrieval input parameter, vegetation optical depth (green color). Variation of blue and red curves is due to the assumed vegetation volume fraction [-] (δ): min=0.001 (blue dotted), max=0.9 (blue dashed), mean (red solid & point) and median (blue dash-dotted & cross) are calculated from minimum to maximum values.

In Fig. 3 the mean and median of M_g for the range of δ is close to 0.2, whereas the extremes of δ lead to M_g-values from 0.03 to 0.6. Apparently, the higher δ the more the temporal dynamics of M_g deviate from the ones of VOD. Thus, for high vegetation volume fractions M_g- and VOD-dynamics differ significantly along time.

As δ is arduous to assess with experimental measurements and not known for this study, we calculated the RWC in two ways: first as RWC-M_g according to (1), second as RWC-VOD substituting M_g with VOD in (1). Moreover, we used, in addition to the minimum and maximum of the M_g-time series, the 5th and the 95th percentile as extremes to account for outlier influences. In Fig. 4 the different RWC-curves are shown for the intensive measuring period. As the extreme values, needed in (1), are taken, in the moment, from the entire time series (April-October 2019), diurnal variations might be under-represented and smoothed. This is still under investigation, but after some time increment analysis, one potential improvement is to use the daily (24h) extreme values in (1) (see Fig. 6).

Figure 4 shows that the extremes (min, max) in the M_g and VOD time series are significantly more different than the percentiles (5%, 95%). Thus, the dynamic ranges between the curves differ strongly with a significant reduction when minimum and maximum values serve as extreme values in (1). Furthermore, using VOD instead of M_g for the calculus in (1) has negligible effect when percentiles are applied, and a small effect when minimum and maximum values are used.

Overall, VOD seems to be an appropriate predictor for plant water content in this study setup [4]. This might be the case, since dry biomass and vegetation structure dynamics at Prospect Hill (Harvard Forest), detectible at L-band, are probably low between April and October 2019. In the case of agriculture, like in [6], the growing cycle with its vivid change in phenology, meaning in plant structure, height and biomass, calls for a decomposition of VOD into a plant water and a plant biomass component to calculate RWC in the end.

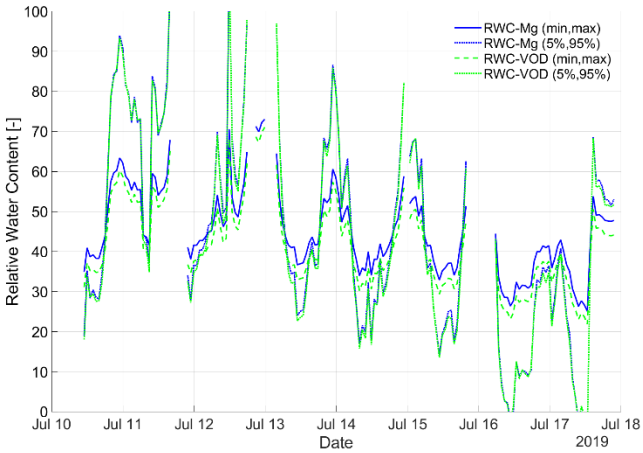

Fig. 4. RWC time series applying minimum and maximum values (min, max) or percentile ranges (5%, 95%) to (1); Blue curves use M_g as input variable in (1), whereas green curves directly apply VOD to (1).

In the final processing step, an effective (as seen by an L-band radiometer system) FWP is calculated from the retrieved RWC-estimates using individual RWC-FWP relationships presented exemplarily in Fig. 2.

In Fig. 5 FWP-estimates are shown for an in situ-linear fitted (gray dashed line in Fig. 2) and for an oak-model-based (blue circles in Fig. 2) relationship between RWC and FWP. Both FWP-estimates cover a different value range of FWP due to their different approach. While the in situ-based estimates range mostly between -10 MPa and -5 MPa, the oak model-based estimates locate between -4 MPa and -1 MPa. Both are compared with in situ xylem water potential measurements of three trees for (parts of) the intensive measurement period. They mainly vary between -5 MPa and zero MPa. It is important to note that in situ measurements for establishing the in situ-fitted RWC-FWP relationship are leaf and branch water potential values (see crosses in Fig. 2, approx. range: -0.3 MPa to -2.3 MPa) and the in situ ones for comparison in Fig. 5 are xylem water potential values (brown solid curve, approx. range: -0.05 MPa to -0.55 MPa). Hence, independent datasets are used for both steps (RWC to FWP conversion & in situ comparison). However, a mismatch in absolute terms might be explicitly introduced in this way.

Furthermore, estimation of an effective FWP from L-band radiometry might not be directly comparable to leaf or xylem water potential measurements of single trees and/or leaves in

the radiometer footprint, as a constant bias between estimates and measurements is apparent in Fig. 5.
Nonetheless, Fig. 5 already indicates the concurrence in temporal trends and diurnal variations between in situ measurements and radiometer-based estimates.

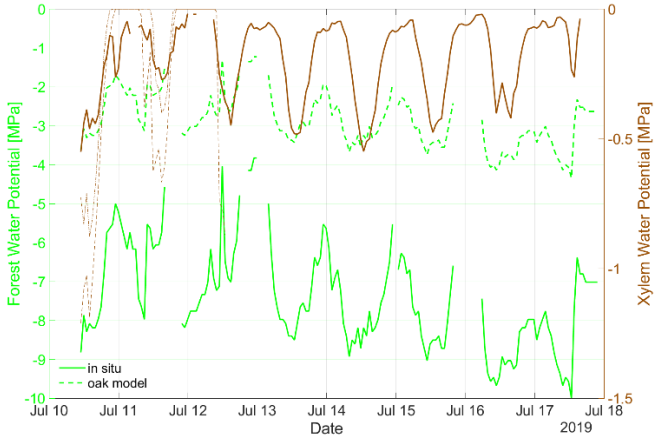

Fig. 5. Time series of FWP-estimates (green color) compared with in situ measurements of xylem water potential of three different trees (brown colored lines) within the L-band radiometer footprint; FWP-estimates are calculated with a linear fit from an in situ-derived (solid line) and an oak model-based (dashed line) RWC-FWP relationship (see Fig. 2).

In contrast to Fig. 5, FWP is estimated in Fig. 6 with a specifically adapted (k_1=*25*, k_2=*31*, FWP_{min}=*-0.55 [MPa]*) slow change sigmoidal model (see cyan curve in Fig. 2 as one example and (2) for calculus) and using daily (24h) $M_{g_{min}}$- and $M_{g_{max}}$-references.

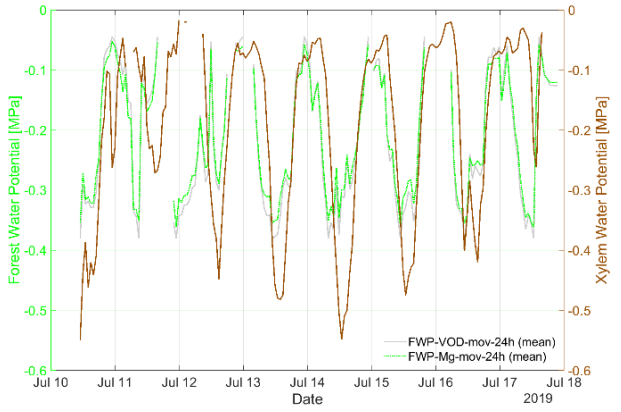

Fig. 6. Comparison of in situ measurements (brown curve) and radiometer-based estimates (green (M_g) and gray (VOD) curves) of FWP; FWP-values are calculated with (2) using a slow sigmoidal model (see Fig. 2) adapted with k_1=25 and k_2=31; FWP_{min}=-0.55 [MPa] and daily (24h) $M_{g_{min}}$ and $M_{g_{max}}$ for RWC calculus.

Here, the bias between measurements and estimates is removed by the adapted parameterization for the study case. Nonetheless, the diurnal variations are significantly smaller in the estimated cases, seeing the full canopy and not only the xylem, where in situ reference is measured. This mismatch is almost indifferent (only small offset), if M_g or VOD is used as predictor variable. Moreover, the difference of mean or median of M_g due to variation of the vegetation volume fraction in the M_g-retrieval only leads to a marginal shift of values (only FWP of M_g (mean) is shown in Fig. 6).
Figures 5 and 6 are first comparisons. A validation of radiometer-based estimates with in situ measurements of water potential will be presented in the conference presentation, looking into the different tree compartments (leaf & xylem) as well as into diurnal until seasonal intervals of the temporal water potential dynamics. Analyses from April to October 2019 of M_g, RWC and FWP will be presented using a variety of RWC-FWP relationships.

6. REFERENCES

[1] D. Entekhabi, et al., „The soil moisture active passive (SMAP) mission," *Proceedings of the IEEE*, *98*(5), pp.704-716, 2010.
[2] T.H. Van den Honert, "Water transport in plants as a catenary process,". *Discussions of the Faraday Society*, *3*, pp.146-153,1948.
[3] D. Entekhabi, et al., "SMAP handbook–soil moisture active passive: Mapping soil moisture and freeze/thaw from space," 2014.
[4] N. Holtzman, et al., "L-band vegetation optical depth as an indicator of plant water potential in a temperate deciduous forest stand," *Biogeosciences Discussions*, pp.1-26, 2020.
[5] N. Holtzman, A. G. Konings, A. Roy, and A. Colliander, "*SMAPVEX19-21 Massachusetts Vegetation Optical Depth, Version 1*," [All]. Boulder, Colorado USA. NASA National Snow and Ice Data Center Distributed Active Archive Center. doi: https://doi.org/10.5067/2PZJDURUJLWF. [12.12.2020].
[6] T. Jagdhuber, et al., "Assessing vegetation water potential of winter wheat on field-scale by ground-based L-band radiometry," MicroRAD conference, Florence, Italy, November, 16-20, 2020.
[7] A. Colliander, et al., "SMAP Detects Soil Moisture Under Temperate Forest Canopies," *Geophysical Research Letters*, *47*(19), p.e2020GL089697, 2020.
[8] T.L. Rowlandson, et al., "Capturing agricultural soil freeze/ thaw state through remote sensing and ground observations: A soil freeze/thaw validation campaign," *Remote Sensing of Environment*, *211*, pp.59-70, 2018.
[9] A. Roy, et al., "L-Band response to freeze/thaw in a boreal forest stand from ground-and tower-based radiometer observations," *Remote Sensing of Environment*, *237*, p.111542, 2020.
[10] T. Meyer, et al., "Estimating gravimetric water content of a winter wheat field from L-band vegetation optical depth,". *Remote Sensing*, *11*(20), p.2353, 2019.
[11] R.E. Smart, and G.E. Bingham, "Rapid estimates of relative water content," *Plant physiology*, *53*(2), pp.258-260, 1974.
[12] R. Zweifel, H. Item, and R. Häsler, "Link between diurnal stem radius changes and tree water relations," *Tree physiology*, *21*(12-13), pp.869-877, 2001.
[13] A.G. Konings, et al., "Macro to micro: microwave remote sensing of plant water content for physiology and ecology," *New Phytologist*, *223*(3), pp.1166-1172, 2019.
[14] G. Mirfenderesgi, et al., "Tree level hydrodynamic approach for resolving aboveground water storage and stomatal conductance and modeling the effects of tree hydraulic strategy," *Journal of Geophysical Research: Biogeosciences*, *121*(7), 1792-1813, 2016.
[15] F.B. Sullivan, et al., "Comparison of lidar-and allometry-derived canopy height models in an eastern deciduous forest," *Forest Ecology and Management*, *406*, 83-94, 2017.